



Structural Basis for the Persistence of Homing Endonucleases in Transcription Factor IIB Inteins

Hideo Iwai¹, Kornelia M. Mikula¹, Jesper S. Oeemig^{1,4}, Dongwen Zhou^{2,5}, Mi Li^{2,3} and Alexander Wlodawer²

1 - Research Program in Structural Biology and Biophysics, Institute of Biotechnology, University of Helsinki, P.O. Box 65, Helsinki FIN-00014, Finland

2 - Macromolecular Crystallography Laboratory, National Cancer Institute, Frederick, MD 21702, USA

3 - Basic Science Program, Leidos Biomedical Research, Frederick National Laboratory for Cancer Research, Frederick, MD 21702, USA

Correspondence to Hideo Iwai and Alexander Wlodawer: hideo.iwai@helsinki.fi; wlodawer@nih.gov

<https://doi.org/10.1016/j.jmb.2017.10.016>

Edited by Dan Tawfik

Abstract

Inteins are mobile genetic elements that are spliced out of proteins after translation. Some inteins contain a homing endonuclease (HEN) responsible for their propagation. Hedgehog/INTein (HINT) domains catalyzing protein splicing and their nested HEN domains are thought to be functionally independent because of the existence of functional mini-inteins without HEN domains. Despite the lack of obvious mutualism between HEN and HINT domains, HEN domains are persistently found at one specific site in inteins, indicating their potential functional role in protein splicing. Here we report crystal structures of inactive and active mini-inteins derived from inteins residing in the transcription factor IIB of *Methanococcus jannaschii* and *Methanocaldococcus vulcanius*, revealing a novel modified HINT fold that might provide new insights into the mutualism between the HEN and HINT domains. We propose an evolutionary model of inteins and a functional role of HEN domains in inteins.

© 2017 Published by Elsevier Ltd.

Introduction

RNA splicing and alternative splicing are highly regulated processes during gene expression in higher organisms, leading to diverse gene transcripts coding for multiple proteins from a single gene [1]. Limited numbers of genes found in genomes of higher organisms could thus result in much larger proteomic diversity created by RNA alternative splicing. Indeed, a large fraction of the protein-coding genes of multicellular organisms is alternatively spliced [2]. In addition to the molecular diversity created at the RNA level, alternative splicing at the protein level has been recently discovered, in which up to four different molecular species could be produced from intermolecular protein splicing between two precursor proteins (two coding genes) [3]. This alternative splicing at the protein level is mediated by another class of intervening sequences called inteins (*internal protein*) and is termed intein-mediated protein alternative splicing (iPAS) [3]. Inteins are parasitic genetic elements inserted into protein-coding genes without

providing any benefits to host proteins, as well as to host organisms [4,5]. Inteins catalyze self-removal from the intervening host proteins after protein translation, concomitantly producing the functional intein-less protein by introducing a peptide bond between the interrupted host protein fragments (Fig. 1) [4,5]. Until the discovery of iPAS [6,7] protein splicing was thought to take place only as an intramolecular reaction or as a bi-molecular *trans*-reaction by split inteins. Inteins are particularly prevalent in archaea, are present in half of their genomes, and have been found only in unicellular organisms [4,8]. They have generally been considered to be pure parasitic proteins with no biological function, but several functional roles have been suggested for specific inteins, such as environmental sensors [9–12]. The biological function of iPAS is not only unknown but also challenging to identify in nature because protein splicing does not leave any mark on the mature host proteins and is impossible to trace back to the originating genes from the alternatively spliced products [3].

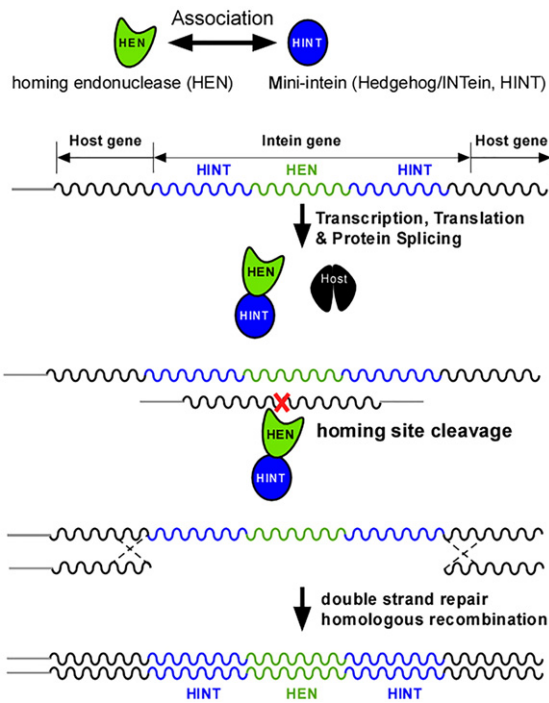


Fig. 1. The homing mechanism of inteins. Host gene exons and products are in black. HEN stands for homing endonuclease (green). HINT stands for Hedgehog/INTEIN domain (blue).

Protein splicing is catalyzed by inteins that share a common structural Hedgehog/INTEIN (HINT) fold [13]. Many inteins are bi-functional, containing not only a HINT domain for protein splicing but also a homing endonuclease (HEN) domain, which is considered to

be responsible for their propagation by horizontal gene transfer (HGT) (Fig. 1) [5,14,15]. The existence of natural mini-inteins without HEN domains and engineered functional mini-inteins without the nested HEN domains suggests that protein splicing and HEN domains are functionally independent [16–19]. Inteins are found in conserved regions of their host proteins near the active sites. The insertion at the essential sites ensures the survival of inteins by making it difficult to remove them [5]. Interestingly, HEN domains are found in only one specific site in many inteins, which also corresponds to the split site found in naturally split inteins. One of the remaining questions in the evolution of inteins is why HEN domains persist only at one specific insertion site when there is no mutualism between HEN and HINT domains (Fig. 1) [20]. Degenerated HEN domains without endonuclease activity persist against genetic drifts within inteins, suggesting that some parts of the HEN domain could be important for protein-splicing reaction by the intein, or contribute to its overall architecture [20,21].

We previously found that the *Methanococcus jannaschii* intein (*Mja*TFIIB) is very efficient in *cis*-splicing using an *Escherichia coli* system [22]. However, a *Mja*TFIIB mini-intein without the HEN domain turned out to be splicing-deficient, supporting the hypothesis that its HEN domain could play a critical role in the splicing process [20,21]. Paradoxically, the inactive engineered *Mja*TFIIB mini-intein without the HEN domain could still induce iPAS in the presence of a split precursor protein containing the C-terminal 53-residue fragment of the *Mja*TFIIB intein [3]. This observation contradicts any structural role of the HEN domain in *Mja*TFIIB intein because protein splicing of the engineered *Mja*TFIIB mini-intein can be

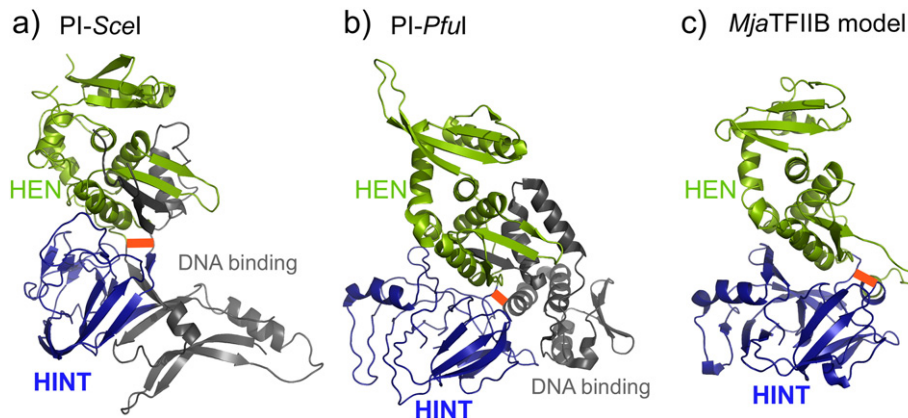


Fig. 2. Design of *Mja*TFIIB mini-intein. Structures of PI-Scel (a), PI-*Pful* (b), and the modeled full-length *Mja*TFIIB intein (c). HINT domains and HEN domains are colored in blue and green, respectively. The DNA binding domain of PI-Scel and the possible DNA-contacting domain of PI-*Pful* are shown in gray. Red thick lines illustrate possible polypeptide linkers to detach HEN domains from HINT domains.

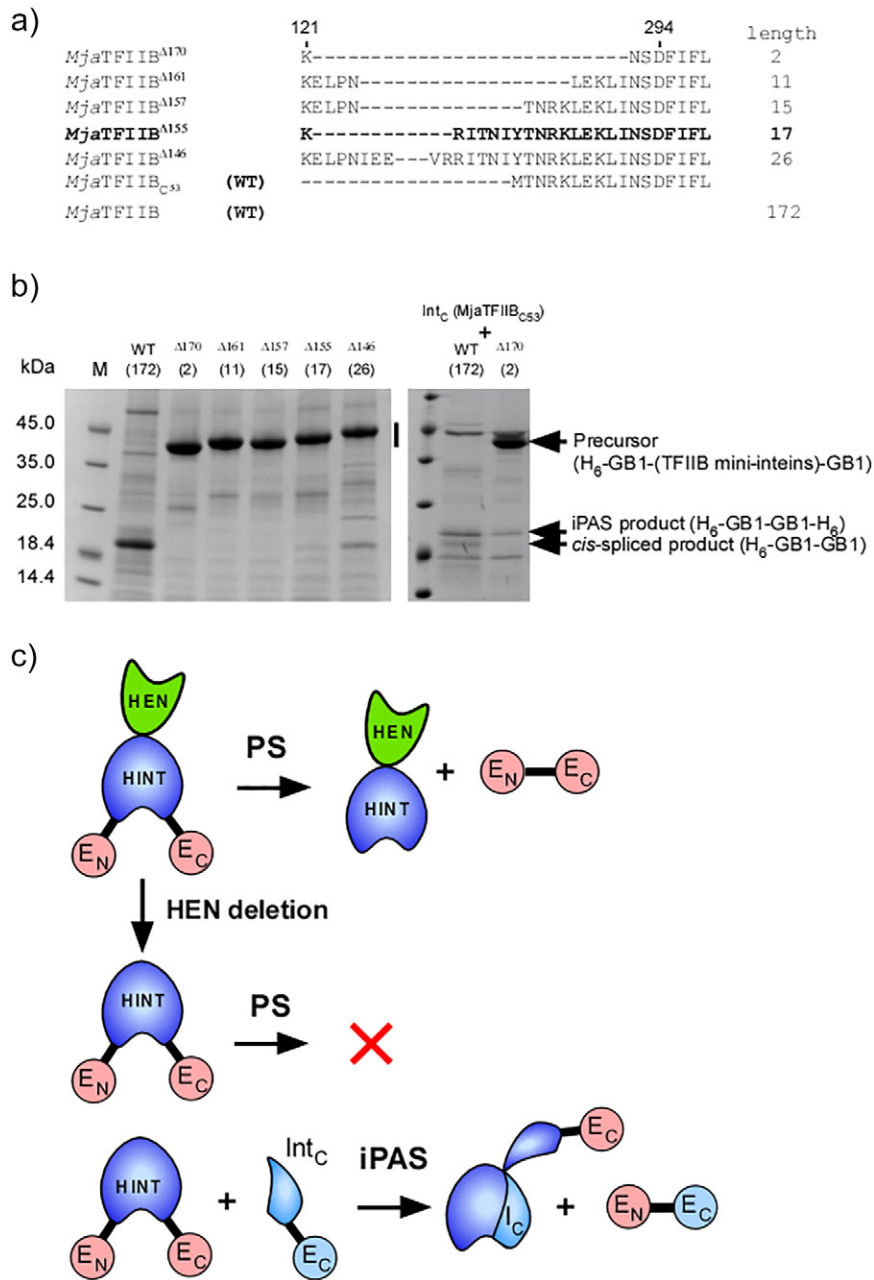


Fig. 3. SDS-PAGE analysis of *cis*-splicing and protein alternative splicing (iPAS) of the full-length *Mja*TFIIIB intein and engineered *Mja*TFIIIB mini-inteins. (a) The sequence alignment of the loop region among the engineered *Mja*TFIIIB mini-inteins and the split intein. The numbers of amino acid residues deleted are indicated in superscript with the name of inteins. The lengths of the loop between residue 121 and 294 are indicated at the right side. WT stands for the wild-type sequence. C53 in subscript indicates the C-terminal 53 residue of the intein. (b) SDS-PAGE analysis of the elution fractions from IMAC purification using the N-terminal His-tag in the precursor protein for *cis*-splicing and alternative splicing. In the left panel, the vertical bar indicates the region where bands of unreacted *cis*-splicing precursor proteins are expected. The right panel shows SDS-PAGE analysis of the elution fractions from co-expression of the C-terminal split intein fragment (*Mja*TFIIIB_{C53}-GB1-H₆) with the *cis*-splicing precursors indicated at the top. Arrows indicate the position of a precursor protein, the band from iPAS product H₆-GB1-GB1-H₆, and the band corresponding to the *cis*-spliced product of H₆-GB1-GB1. M stands for molecular weight markers. The numbers within brackets show the numbers of residues between residue 121 and 294. (c) A cartoon presentation of the effects of the HEN domain (in green) on *cis*-splicing (PS) by HINT domain (in blue) and co-expression of the C-terminal split intein fragment (Int_C). HEN deletion results in a *cis*-splicing deficient intein, which can be partially activated by iPAS with an intein fragment (I_C).

activated in the complete absence of the HEN domain by iPAS. Thus, the origin of the mutualism between HINT and HEN domains in *Mja*TFIIB intein, if any, is still enigmatic.

Here we report the structures of an inactive *Mja*TFIIB mini-intein and a partially active TFIIB mini-intein from *Methanocaldococcus vulcanius* M7 (*Mvu*), elucidated by X-ray crystallography. The structure of *Mja*TFIIB mini-intein revealed a novel HINT fold with an additional β -strand in the core of the HINT domain. Furthermore, protein engineering of mini-inteins from *Mja*TFIIB and *Mvu*TFIIB inteins indicated the importance of the length of the loop, which is invisible in the crystal structure of the functional *Mvu*TFIIB mini-intein. A structural comparison between the two mini-variants of the TFIIB inteins suggests the plasticity or flexibility in the HINT domains. Our results also indicate that there are dynamic features associated with the HINT domain of TFIIB inteins that significantly contribute to the protein-splicing activity. We discuss the functional and evolutionary roles of the HEN domains in inteins and propose a mutualism model between the HEN and HINT domains.

Results

Modeling of *Mja*TFIIB mini-inteins

Small, highly efficient inteins without HEN domains are preferred as protein engineering tools, for example, for protein ligation [18]. TFIIB intein from *M. jannaschii* (*Mja*TFIIB intein) exhibits efficient *cis*-splicing activity in *E. coli* and is smaller than canonical inteins with a HEN domain, such as *Sce*VMA intein and PI-*Pful* [22–24]. Canonical inteins, exemplified by *Sce*VMA intein, typically consist of about 450 residues because of the insertion of a LAGLIDADG-family HEN domain into the HINT fold [25]. We were initially interested in rationally engineering robust *Mja*TFIIB mini-inteins with only the HINT domain, retaining the efficient splicing activity, based on the sequence homology. The homology search using the *Mja*TFIIB intein sequence identified a putative endonuclease domain within *Mja*TFIIB intein, but *Mja*TFIIB intein comprises only 335 residues, which is about 100 residues smaller than *Sce*VMA intein. A BLAST

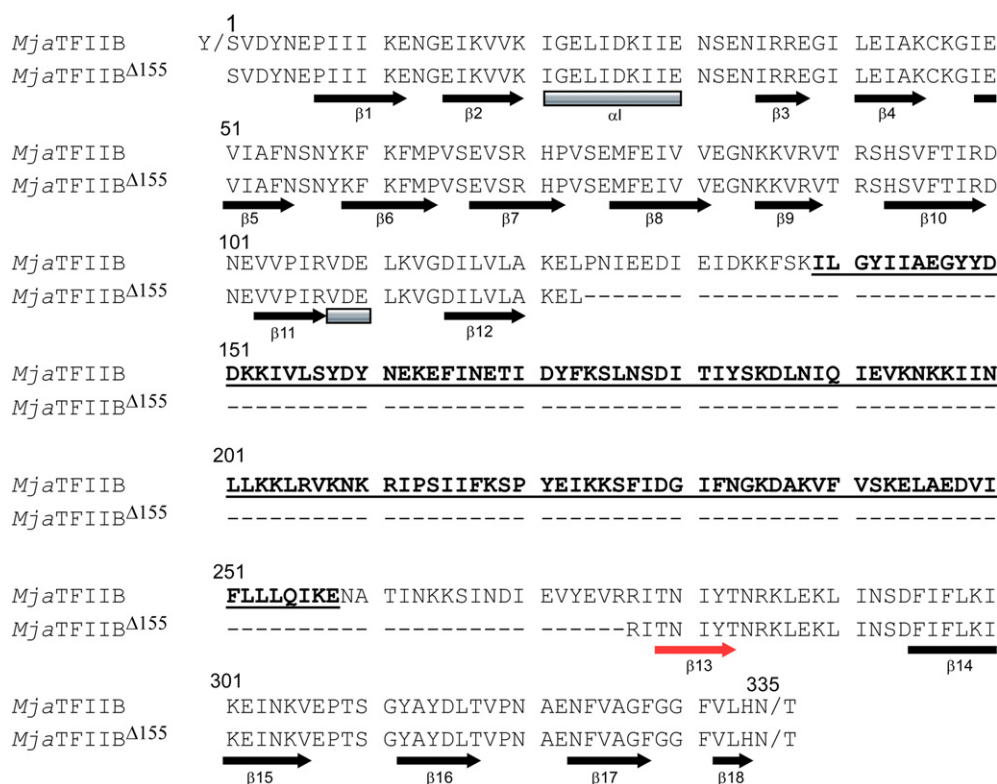


Fig. 4. The sequence comparison of the full-length *Mja*TFIIB intein and *Mja*TFIIB Δ 155 mini-intein with the secondary structures. The secondary structures identified in the crystal structure of *Mja*TFIIB mini-intein (*Mja*TFIIB Δ 155) are shown with arrows (β -sheets) and rectangles (helices). The region of a putative endonuclease domain of *Mja*TFIIB intein is in bold and underlined. The unique β -strand (β 13) identified in the structure of *Mja*TFIIB mini-intein (*Mja*TFIIB Δ 155) is indicated with arrow colored in red.

search against the Protein Data Bank (PDB) identified PI-*Pkoll* (PDB id: 2cw7) and PI-*Pful* (PDB id: 1dq3) as the inteins with two highest homologies

(Supplementary Fig. 1) [24,26]. We used PI-*Pful* as the template to model a three-dimensional structure of *Mja*TFIIB intein for designing mini-inteins (Fig. 2).

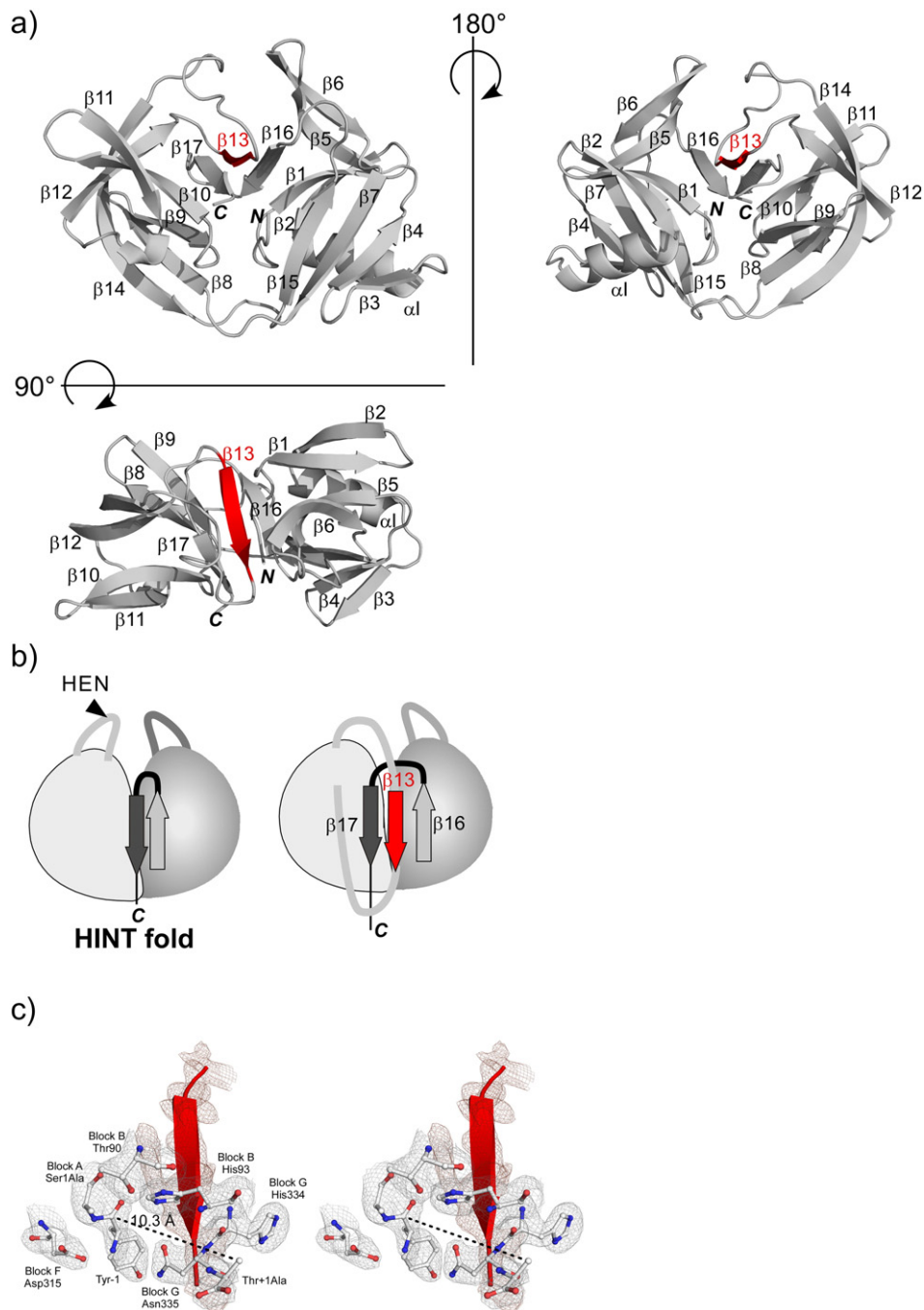


Fig. 5. The crystal structure of *Mja*TFIIB mini-intein (*Mja*TFIIB Δ^{155}). (a) Schematic drawings of the crystal structure of *Mja*TFIIB Δ^{155} from three different orientations. The unusual β -strand (β 13) insertion is colored in red. *N* and *C* stand for N- and C-termini, respectively. (b) Schematic illustrations of the canonical HINT fold and the novel HINT fold observed in *Mja*TFIIB Δ^{155} with the last two β strands (dark and light gray) and the unusual β -strand (β 13) insertion (red). (c) A stereoview of the active site together with the inserted β -strand (β 13) in red. The distance between the carbonyl carbon atom of Tyr-1 and C β atoms of Ala +1 is shown in dotted line. The final electron density map, contoured at 1.0 σ -level, is shown for the selected residues (in gray) and for the β 13-strand (in dark pink).

Mini-inteins containing only the HINT fold without deterioration of the protein-splicing activity have been successfully engineered by removing HEN domains, for example, *MtuRecA*, *SspDnaB*, and *NpuDnaB* inteins, among others, suggesting that the HEN domains are not essential for protein splicing activity [16,18,19].

We first attempted to create a mini-intein from *MjaTFIIB* intein by retaining only the residues corresponding to the HINT fold, analyzing the homology model created from the alignment with *PI-Pful* (Fig. 2; Supplementary Fig. 1). We expected that the inserted HEN domain (170 residues) might be safely removed from *MjaTFIIB* intein without disrupting the HINT fold, as it was successfully done with other inteins. However, the engineered

MjaTFIIB mini-intein (*MjaTFIIB*^{Δ170}) turned out to be deficient in *cis*-splicing, although alternative protein splicing was observed with a C-terminal split fragment of *MjaTFIIB* intein by iPAS without the HEN domain (Fig. 3) [3]. This observation induced us to investigate the three-dimensional structure of *MjaTFIIB* intein further. This result might suggest that the three-dimensional structure could completely differ from other known inteins, from which HEN domains can be removed without affecting splicing activity. To understand the structural basis for the splicing deficiency of the engineered *MjaTFIIB* mini-intein (*MjaTFIIB*^{Δ170}), we attempted to determine the three-dimensional structures of various mini-inteins of *MjaTFIIB* intein and of its homolog.

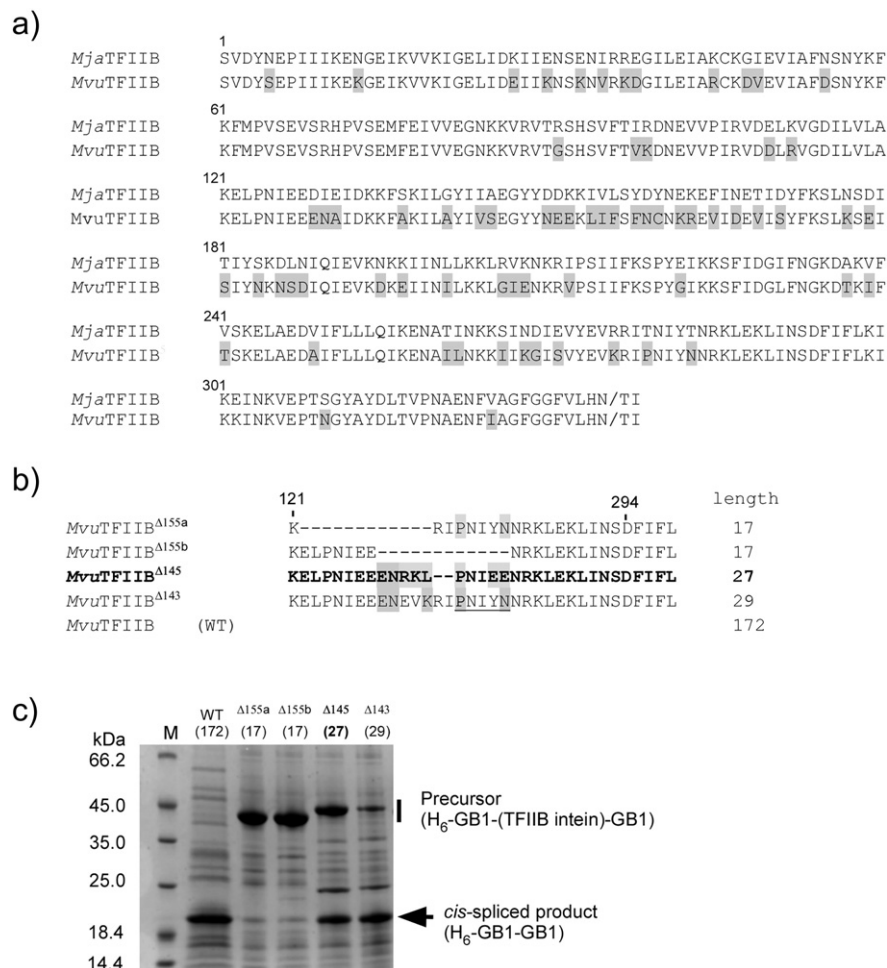


Fig. 6. *MvuTFIIB* intein and *MvuTFIIB* mini-inteins. (a) A comparison of the primary structures of *MjaTFIIB* and *MvuTFIIB* inteins. (b) The sequence alignment of the loop region of the engineered *MvuTFIIB* mini-inteins. The numbers of amino acid residues removed from the loop region are indicated in superscript together with the name of the intein. The lengths of the loop between residue 121 and 294 are indicated at the right side. (c) SDS-PAGE analysis of the elution fractions from IMAC using the N-terminal His-tag in the precursor protein. The vertical bar indicates the region where bands of unreacted precursor proteins are expected. An arrow indicates the band corresponding to the *cis*-spliced product of *H₆-GB1-GB1*. M stands for molecular weight marker. Numbers within brackets indicate the numbers of the remaining residues between residues 121 and 294.

Deletion variants of *Mja*TFIIIB inteins

We employed the strategy of engineering mini-inteins by eliminating their HEN domains based on sequence alignment that we used previously [18,27]. However, the first engineered mini-intein derived from *Mja*TFIIIB intein (*Mja*TFIIIB Δ 170) did not catalyze *cis*-splicing using a model system that utilized the B1 domain of IgG binding protein G (GB1) as flanking exteins (Fig. 3) [3]. We slightly modified the deletion in the loop where the presumed HEN domain is located by extending the connecting loop length (Fig. 3). To our surprise, further elongation of the loop in the *Mja*TFIIIB mini-inteins offered little improvement of the splicing activity, implying that the deficiency in protein

splicing is not merely due to the insufficient loop length or constraints introduced by the deletion, but that other factors might play critical roles. This observation suggested that there could be some mutualism between the HEN and HINT domains (Fig. 3).

Unexpected modification of the HINT fold in the *Mja*TFIIIB Δ 155 mini-intein

Despite many attempts to crystallize the full-length *Mja*TFIIIB intein and various *Mja*TFIIIB mini-inteins, we could obtain crystals for only one of them, namely, *Mja*TFIIIB Δ 155 (Figs. 3 and 5). Although *Mja*TFIIIB Δ 155 was deficient in *cis*-splicing in our model *cis*-splicing *E. coli* system, we succeeded in solving its three-

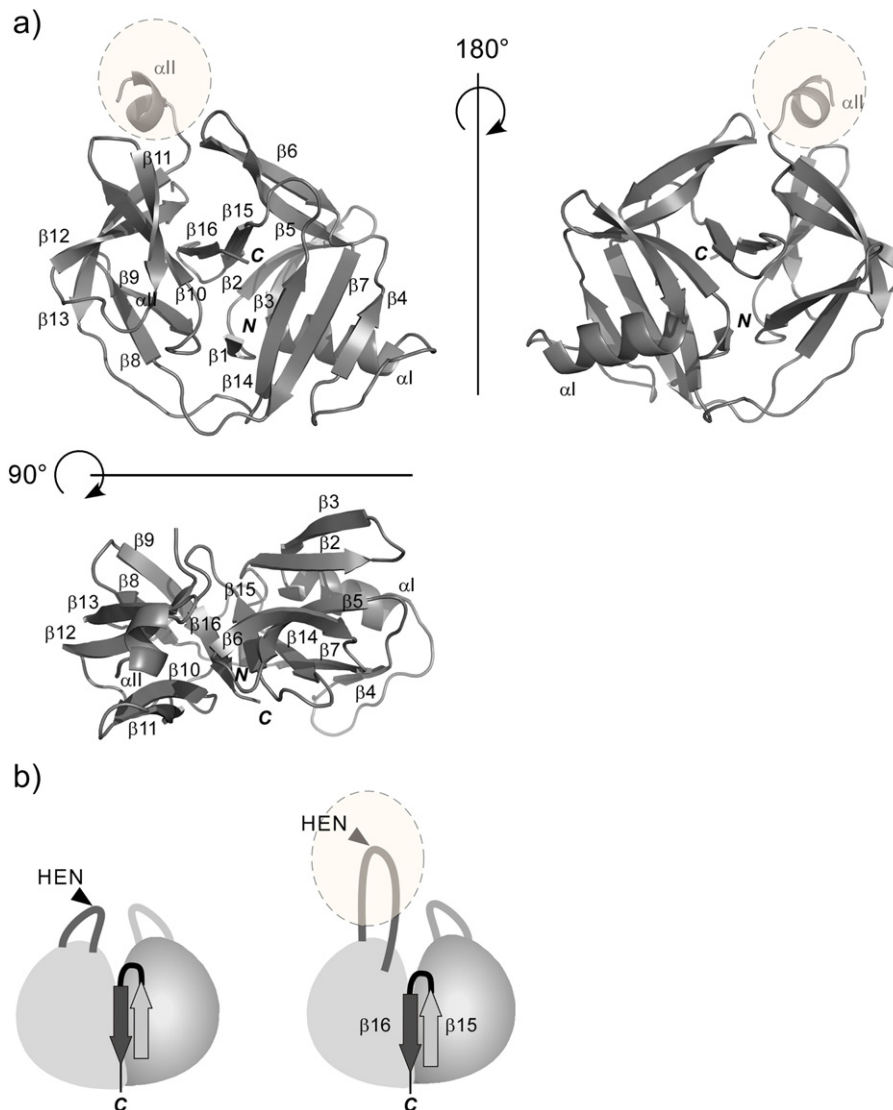


Fig. 7. The crystal structure of *Mvu*TFIIIB mini-intein (*Mvu*TFIIIB Δ 145). (a) Schematic drawings of the crystal structure of *Mvu*TFIIIB Δ 145 from three different orientations as in Fig. 5. Shadowed dashed circles indicate the HEN-insertion region lacking the electron density. (b) Schematic illustrations of the canonical HINT fold and the HINT fold in *Mvu*TFIIIB Δ 145 with the HEN insertion site indicated by arrowheads and the HEN insertion loop by a shadowed dashed circle.

dimensional structure at 2.0-Å resolution (Figs. 3 and 5, Table 1). The structure of *Mja*TFIIB^{Δ155} that resulted from the final refinement contains two protein molecules, six dioxane molecules, one MES molecule, 14 glycerol molecules, 10 ammonium ions, and 194 water molecules in the asymmetric unit. In chain A, 182 out of 185 residues have been modeled, but the first 3 N-terminal residues have not been included due to the complete lack of electron density. In chain B, 183 out of 185 residues have been modeled, with the first 2 N-terminal residues invisible. The structures of the two molecules in the asymmetric unit are very similar except for one loop region (residues 58–65), in which the difference is relatively large (3.8 Å for the Cα of Asn61). However, this loop region is involved in crystal contacts. The root mean square deviation (RMSD) between these two monomers is 0.58 Å for the aligned backbone atoms.

Surprisingly, *Mja*TFIIB^{Δ155} revealed a novel, modified HINT fold, having an extra β-strand in the core near the splicing site (Figs. 4 and 5). The structure of *Mja*TFIIB^{Δ155} can be superimposed well with the search model, which was created based on PI-*Pfull* intein, confirming that it is similar to the HINT fold except for the inserted β-strand (β13) (Figs. 4 and 5)

[13,24]. The RMSD between the search model and the monomer A of *Mja*TFIIB^{Δ155} is relatively large (2.9 Å for 628 pairs of the aligned backbone atoms) due to insertion of an additional β-strand. The loop in *Mja*TFIIB^{Δ155} where a HEN domain typically locates included 17 residues between residues 121 and 294, which folded into a β-strand (β13) and formed an antiparallel β-sheet with β16 (Fig. 5a). The strand β13 is inserted into the core of the HINT fold between the last two β-strands, β16 and β17 (Fig. 5b). However, the distance between the carbonyl carbon atom of the N-terminal scissile bond and Cβ atom of the C-terminal nucleophilic residue of C-extein, which is mutated from Thr to Ala, is 10.3 Å. This distance is not much larger than the corresponding distances observed in a majority of the reported intein structures (8–9 Å), which typically have an open conformation (Fig. 5c) [17,23,27]. We initially assumed that this unusual β-strand insertion might inhibit the splicing activity by disrupting the active site coordination. However, deletion of this β-strand from *Mja*TFIIB^{Δ155} (e.g., *Mja*TFIIB^{Δ157}) did not improve the activity of the *Mja*TFIIB mini-intein (Fig. 3). Therefore, we speculate that this unusual HINT fold of *Mja*TFIIB^{Δ155} is more likely to be accidentally produced as the lowest energy

Table 1. Data collection and structure refinement

Data collection	<i>Mja</i> TFIIB ^{Δ155}	<i>Mvu</i> TFIIB ^{Δ145}
	DIAMOND I04	ESRF ID-30A-3
Space group	P1	C2
Molecules/a.u.	2	2
Unit cell <i>a</i> , <i>b</i> , <i>c</i> (Å); α, β, γ (°)	50.80, 60.12, 42.36; 75.8, 76.9, 77.4	67.25, 108.18, 51.23; 102.4, 90.0, 90.0
Resolution (Å)*	30.00–2.00 (2.07–2.00)	56.73–2.50 (2.67–2.50)
$R_{\text{merge}}^{\dagger}$ (%)	8.5 (72.4)	8.3 (101.1)
No. of reflections (measured/unique)	72,771/30,100	94,954/12,418
$\langle I/\sigma \rangle$	11.6 (1.6)	13.3 (1.9)
Completeness (%)	95.9 (92.5)	99.5 (96.7)
Redundancy	2.4 (2.3)	7.6 (7.8)
Refinement		
Resolution (Å)	28.7–2.0	56.7–2.5
No. of reflections (total/ R_{free})	30,074/945	11,837/580
$R/R_{\text{free}}^{\ddagger}$	0.214/0.261	0.222/0.278
No. atoms		
Protein	2918	2758
Ligands	118	–
Water	194	16
RMSD from ideal		
Bond lengths (Å)	0.007	0.018
Bond angles (°)	1.013	1.957
Ramachandran plot (%)		
Favored	95.3	93.5
Allowed	4.7	4.1
Outliers	0.0	2.4
PDB code	5O9J	5O9I

ESRF, European Synchrotron Radiation Facility.

* The highest resolution shell is shown in parentheses.

$\dagger R_{\text{merge}} = \sum_h \sum_i |I_i - \langle I \rangle| / \sum_h \sum_i I_i$, where I_i is the observed intensity of the i -th measurement of reflection h , and $\langle I \rangle$ is the average intensity of that reflection obtained from multiple observations.

$\ddagger R = \sum |F_o| - |F_c| / \sum |F_o|$, where F_o and F_c are the observed and calculated structure factors, respectively, calculated for all data. R_{free} was defined in Brünger (1992). [41].

state due to the minimization engineering and does not represent the functionally relevant structure of *Mja*TFIIB intein. The interaction between the two pseudo-domains could be weak, thereby accommodating the insertion.

*Mvu*TFIIB mini-intein (*Mvu*TFIIB Δ^{145})

We still wanted to confirm whether the unexpected HINT fold of *Mja*TFIIB Δ^{155} was truly an accidentally trapped conformation resulting from the minimization of *Mja*TFIIB intein, irrelevant for the splicing activity. To answer this question, we investigated another homologous TFIIB intein from *M. vulcanius* M7 (*Mvu*TFIIB intein), exhibiting sequence identity of 78.5% (Fig. 6a and Supplementary Fig. 1), with the hope of solving its crystal structure. We also found that *Mvu*TFIIB mini-intein, for example, *Mvu*TFIIB Δ^{155} , was inactive, like other *Mja*TFIIB mini-inteins with similar loop lengths, preserving the same intolerance of the HEN deletion observed for the *Mja*TFIIB intein (Fig. 6b and c). Unfortunately, we failed to obtain any diffracting crystals for the full-length *Mvu*TFIIB intein and other *Mvu*TFIIB mini-inteins except for *Mvu*TFIIB Δ^{145} . Importantly, this *Mvu*TFIIB Δ^{145} was at least notably active, although the loop region, where the HEN domain was removed, contains an artificial sequence accidentally introduced during the cloning procedure (Fig. 6b). The HEN insertion loop contains 27 residues (between residues 121 and 294). The *Mvu*TFIIB mini-intein with the 29-residue loop (143-residue deletion in the HEN region) in the same location (*Mvu*TFIIB Δ^{143}) was also partially active, suggesting that TFIIB mini-inteins need at least 27–29 residues in this region for *cis*-splicing activity. We determined the structure of *Mvu*TFIIB Δ^{145} at 2.5-Å resolution (Fig. 7, Table 1). The overall structure of *Mvu*TFIIB Δ^{145} reveals a canonical HINT fold of its two molecules in the asymmetric unit but does not share the unusual HINT fold of *Mja*TFIIB Δ^{155} . The Ramachandran plot shows 93.5%, 4.1%, and 2.4% of all residues falling into the most favored, additionally allowed, and generously allowed regions, respectively (Table 1). Inferior statistics of this structure can be attributed to the poorly defined loop regions (Fig. 7a), presumably resulting in lower crystal quality that affected the resolution of diffraction data. We limited modeling of water molecules to only those that were located in very clear electron density. The longer loop at the deleted HEN region is mostly invisible and was thus not modeled, although this longer loop was essential for the splicing activity. This observation suggests that this functionally required loop is flexible to the point of being disordered.

Comparison between *Mja*TFIIB Δ^{155} and *Mvu*TFIIB Δ^{145}

Importantly, the largest difference between the active *Mvu*TFIIB Δ^{145} and inactive *Mja*TFIIB Δ^{155} is

the unusual β -strand (β 13) insertion found in the core of *Mja*TFIIB Δ^{155} . The HINT fold can be divided into two pseudo-domains that presumably resulted from gene duplication during evolution [13]. After superposition of the first pseudo domains (residues 1–75) of the two structures, the overlaid regions (residues 1–75) superimpose well, with an RMSD of 0.51 Å for the backbone atoms. The last β -strand (β 16) in *Mvu*TFIIB Δ^{145} replaces the inserted β -strand (β 13) between β 16 and β 17 in *Mja*TFIIB Δ^{155} (Figs. 7 and 8). In addition, *Mvu*TFIIB Δ^{145} assumes a more closed conformation with a rotation of 36° of the second domain, indicating plasticity between the two pseudo-domains (Fig. 8). However, the distance between the nitrogen atom of Cys1Ala and carbonyl carbon atom of the last residue of Asn is similar in the two structures (9.6 Å for *Mvu*TFIIB Δ^{145} , compared with 9.1 Å of *Mja*TFIIB Δ^{155}). This result indicates the presence of an “open conformation” similar to many reported inteins structures, although *Mvu*TFIIB Δ^{145} lacks the –1 and +1 residues [17,23,24,27]. We believe that the structure of *Mvu*TFIIB Δ^{145} represents better the functional state of the TFIIB inteins than that of *Mja*TFIIB Δ^{155} .

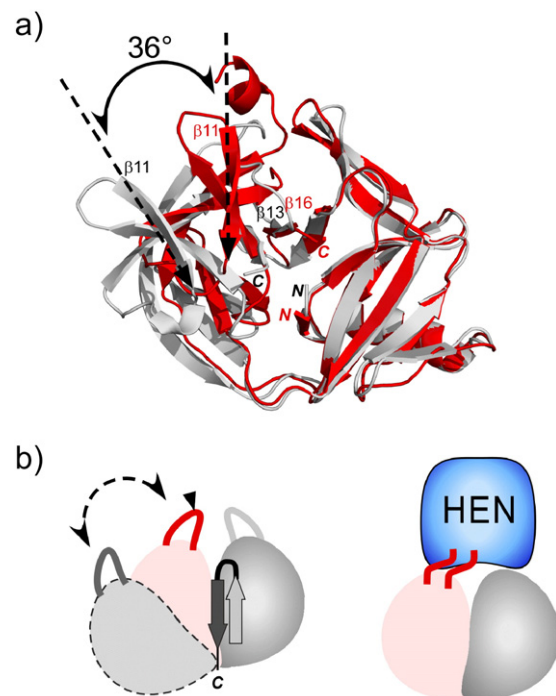


Fig. 8. Comparison of two mini-intein structures of *Mja*TFIIB Δ^{155} and *Mvu*TFIIB Δ^{145} . (a) A superposition of the two coordinates after fitting the backbone atoms of residues 1–75. The angle of β 11 strand of both structures was derived from the superimposed structures and shown. Ribbon drawings of *Mvu*TFIIB Δ^{145} and *Mja*TFIIB Δ^{155} are colored in red and gray, respectively. (b) Schematic illustrations of the two structures highlighting two pseudo-sub-domains and the movement observed for *Mja*TFIIB Δ^{155} (left) and a model with the HEN domain (right).

Discussion

The new crystal structures of the inactive *Mja*TFIIB mini-intein and partially active *Mvu*TFIIB mini-intein (*Mja*TFIIB Δ^{155} and *Mvu*TFIIB Δ^{145}) shed new light on how HEN domains persist in inteins by providing a mutualism between HINT and HEN domains. Many canonical inteins contain a HEN domain that cleaves the DNA sequences near the intein insertion points. Such enzymatic activity has presumably played (or still plays) an important role in the propagation of intein genes by HGT (Fig. 1), similarly to other selfish gene elements such as intron-encoded HENs [28,29].

Minimization engineering of TFIIB inteins by removing the HEN region resulted in unexpected splicing deficiency, unlike in other previously reported engineered mini-inteins [16,18,19]. Nonetheless, the elucidated three-dimensional structures of the engineered TFIIB mini-inteins are in agreement with the structural requirement for active HINT domains (e.g., only 5.6 Å between the carbonyl carbon of residue 121 and nitrogen atom of residue 294 in the structure of *Mja*TFIIB Δ^{155} and 7.9 Å for *Mvu*TFIIB Δ^{145}) (Fig. 2). This agreement between the original homology model and the experimentally determined structure indicates that the distinct lowest energy status found in the crystal structure is not solely responsible for the splicing reaction. We speculate that the folding process and/or structural dynamics of the HEN domain in TFIIB inteins must play a critical role in protein splicing (Fig. 2). The engineered mini-inteins remain inactive despite further modifications of the connecting loop. A longer linker (at least 26 residues between residues 121 and 294) at the HEN insertion site was found to be required for restoring the partial activity of TFIIB inteins (Figs. 3 and 6). Despite the requirement of a longer linker for the function, these residues were invisible in the electron density of *Mvu*TFIIB Δ^{145} , suggesting that this region is disordered/flexible. This observation supports an interpretation that structural dynamics involved with the engineered longer linker and the original HEN domain might play an important role in protein splicing activity, rather than that some parts of the HEN domain contribute to the functional HINT domain architecture. The importance of structural dynamics rather than the structural integration of the HEN domain in the HINT domain could also explain the observed iPAS of *Mja*TFIIB mini-inteins induced by the C-terminal 53-residue fragment of *Mja*TFIIB intein (*Mja*TFIIB_{C53}) without any part of the HEN domain [3] (Fig. 3). It is also in line with the engineered RecA mini-inteins, of which local dynamics could account for the difference in self-cleavage activity [33,34]. A comparison between the inactive *Mja*TFIIB Δ^{155} and active *Mvu*TFIIB Δ^{145} shows inter-domain flexibility between the two pseudo-sub-domains of the HINT fold of TFIIB inteins (Fig. 8). The HEN domains of TFIIB inteins are likely to play a critical role in bringing the two

pseudo-sub-domains into an active conformation or/and controlling the concerted protein splicing reaction steps. Unlike other inteins, the HEN domain of TFIIB inteins might be essential for productive protein folding which is coupled with protein splicing reaction of the HINT domain or for structural dynamics necessary for protein splicing. In other words, the HEN domain of TFIIB inteins could be considered to have the maturase activity to assist proper folding of HINT domains, similar to HEN encoded RNA-maturase encoded in introns [35].

Our studies, as well as studies by others, postulate that HEN-containing inteins can be classified into at least two distinct classes. One of them is the group of inteins in which HEN and HINT domains are functionally independent and have developed little or no mutualism between them. In that case, the HEN domains can be easily removed without any loss of the protein splicing activity [36]. One might consider that these inteins appeared by recent invasions of mini-inteins by a HEN domain (Fig. 9). Therefore, they are still mostly tolerant to the loss of HEN domains with no interference to protein splicing. The other class consists of inteins that have already developed some mutualism between the HINT and HEN domains, with their splicing activities becoming largely dependent on the existence of the inserted HEN domain. Adaptation of HEN domains to the invaded inteins could provide persistence or maintenance of HEN domains within inteins by the mutualism. In the case of TFIIB intein, the function of HEN domain might be to assist folding of the HINT domain to a functional conformation of TFIIB inteins, thereby promoting protein splicing. This function is analogous to RNA-maturase as found in introns encoding HEN, which promotes intron splicing [35]. For HINT domains, such mutualism could apparently ensure the propagation of intein genes by HGT [4,20]. For HEN domains, the mutualism could make it harder to eliminate them from intein genes, because a loss of the active or inactive HEN domain would lead to impaired splicing activity required for survival of host organisms, thereby ensuring the survival of the HEN domains in inteins. It might be possible to consider that these inteins have been invaded with a HEN domain much earlier and developed the mutualism by co-evolution (Fig. 9). In this scenario, naturally existing mini-inteins are possible survivors of ancestral mini-inteins that did not develop any mutualism with HEN domains during homing cycles and are still lacking a HEN domain (Fig. 9).

To the best of our knowledge, all of the HEN-containing inteins share, without any exception, only one common insertion site for their HEN domains which also coincides with the naturally occurring split site (C35 site, according to the *Npu*DnaE-based numbering system that we previously proposed), although HEN domains could, in principle, invade any sites of inteins during the homing cycle [39]. It is still

template. pBHDuet50K was accidentally created by incorporation of the oligonucleotides twice. *MvuTFIIB*^{Δ143} (pBHDuet64) was constructed from pBHDuet33 using the two oligonucleotides of I581: 5'-GAATATTGAAGAAGAGAATGAAGTAAAGA-GAATACCC and I582: 5'-GGGTATTCTCTTACTT-CATTCTCTTCTTCAATATTC.

Analysis of *cis*-splicing by mini-inteins

Cis-splicing by *MjaTFIIB* and *MvuTFIIB* mini-inteins was analyzed by expressing the constructs described above. *E. coli* strain ER2566 (New England Biolabs) was transformed with each plasmid carrying a mini-intein and plated on LB-agar plates supplemented with 25 μg/ml kanamycin at 37 °C. Five milliliters of LB medium supplemented with a final concentration of 25 μg/ml kanamycin was inoculated with a single colony and incubated with vigorous shaking at 250 rpm overnight at 37 °C. Five milliliters of the overnight culture was diluted into 45 ml of fresh LB medium supplemented with a final concentration of 25 μg/ml kanamycin and incubated at 37 °C with shaking at 250 rpm. When OD₆₀₀ reached 0.6, the mini-intein was induced with a final concentration of 1 mM isopropyl-β-D-thiogalactoside for 3 h at 37 °C. The induced cells were harvested by a 10-min centrifugation at 4000 rpm, 4 °C and re-suspended in 4 ml of 50 mM sodium phosphate buffer (pH 8.0) and 300 mM NaCl. The half of the re-suspended cells was lysed by sonication. The His-tagged protein was purified using a Ni-NTA spin column according to the manufacturer's protocol (Qiagen). The elution from the spin-column was diluted with two-fold SDS loading buffer containing 1 mM dithiothreitol and analyzed on 18% SDS polyacrylamide gels after Coomassie Blue R (GE Healthcare Life Sciences) staining.

Cloning, expression, and purification of *MjaTFIIB*^{Δ155}

The gene of *MjaTFIIB*^{Δ155} mini-intein with C1A mutation for structure determination was amplified from pSADuet779 as the template using the two oligonucleotides of HK803: 5'-ATGGATCCGGTGG ATATGCTGTTGATTACAACGAAC and HK804: 5'-TCGGTACCTTAGGCGTTGTGTAATACAAA TCCTC, and cloned between *Bam*HI and *Kpn*I site of pHYRSF53, resulting in plasmid pSCFRSF131 bearing *MjaTFIIB*^{Δ155} as His-tagged SUMO fusion protein [42].

E. coli strain ER2566 (New England Biolabs) was transformed with the plasmid pSCFRSF131 carrying H₆-SUMO-*MjaTFIIB*^{Δ155} (C1A). Fifty milliliters of LB medium supplemented with a final concentration of 25 μg/ml kanamycin was inoculated with a single colony and incubated with vigorous shaking at 250 rpm overnight, at 30 °C. The overnight culture was diluted into 2 l of fresh LB medium supplement-

ed with a final concentration of 25 μg/ml kanamycin and incubated at 37 °C with shaking at 250 rpm. When OD₆₀₀ reached 0.6, *MjaTFIIB*^{Δ155} was induced with a final concentration of 1 mM isopropyl-β-D-thiogalactoside for 3 h at 37 °C. The induced cells were harvested by a 10-min centrifugation at 1500 rpm, 4 °C, and re-suspended in 15 ml with lysis buffer (50 mM sodium phosphate buffer (pH 8.0) and 300 mM NaCl). The cells were flash-frozen in liquid nitrogen, and stored at -74 °C. The SUMO fusion was purified by immobilized metal ion affinity chromatography (IMAC) using a 5-ml HisTrap FF column (GE Healthcare Life Sciences) following the previously published protocol for purification of the SUMO-fusion proteins [43]. *MjaTFIIB*^{Δ155} mini-intein with C1A mutation was collected from flow-through fractions from the second IMAC after ubiquitin-like-specific protease 1 protease digestion and dialyzed against 2 l of MilliQ water overnight at 4 °C. The protein was concentrated to 447 μM using an ultracentrifugation device, and flash-frozen in liquid nitrogen for storage at -74 °C.

Cloning, expression, and purification of *MvuTFIIB*^{Δ145} for structure determination

The gene of *MvuTFIIB*^{Δ145} mini-intein with C1A mutation was amplified by PCR from the pBHDuet50F plasmid using the two oligonucleotides of I583: 5'-ATGGATCCGGTGGTACGCTGTTGATTA TAGCGAACC and HK804: 5'-TCGGTACCTTA GGCGTTGTGTAATACAAATCCTC. The amplified gene was inserted into pHYRSF53 using *Bam*HI and *Kpn*I sites to make the SUMO-fusion protein, resulting in pBHRSF63 [43].

The SUMO-fusion bearing *MvuTFIIB*^{Δ145} mini-intein with C1A mutation was expressed and purified following the protocol above [43]. The protein was further purified by gel filtration chromatography. The protein solution was concentrated using an ultracentrifugation device to a volume of 2 ml and loaded onto Superdex75 size exclusion chromatography column (GE Healthcare Life Sciences) with Tris-buffered saline buffer (pH 7.4). The monodisperse peak fractions containing *MvuTFIIB*^{Δ155b} were dialyzed against two liters of MilliQ water overnight at 4 °C. The protein was concentrated to 802 μM using an ultracentrifugation device, and flash-frozen in liquid nitrogen for storage at -74 °C.

Crystallization of *MjaTFIIB*^{Δ155} and *MvuTFIIB*^{Δ145}

A 447 μM solution of *MjaTFIIB*^{Δ155} and 802 μM solution of *MvuTFIIB*^{Δ145} were used for crystallization trials. Drops of 200 nl (100 nl of protein solution and 100 nl of screen solution) were set up in 96-well MRC (Molecular Dimensions) crystallization plates

using a Mosquito LCP® (TTP Labtech, UK). Helsinki Random I and II (HRI and HRII) screens[†], which are the local modifications of the classic sparse matrix screens yielded initial hits [44]. Optimization grid screens were designed based on the initial hits and crystal growth was improved. The final growth conditions for the diffracting crystals were 0.1 M Mes buffer (pH 6.5), 10% dioxane, and 1.6 M ammonium sulfate for *Mja*TFIIB^{Δ155}, and 0.2 M calcium chloride and 20% PEG 3350 for *Mvu*TFIIB^{Δ145}. Glycerol (25%) was added for *Mja*TFIIB^{Δ155} on top of the drop, which served as a cryoprotectant when flash-freezing crystals in liquid nitrogen. For *Mvu*TFIIB^{Δ145}, sufficient cryoprotection was obtained with 20% PEG 3350 present in crystallization drop.

Diffraction data collection and processing

Diffraction data for the crystal of *Mja*TFIIB^{Δ155} mini-intein were collected in a single pass on beamline I04 at the Diamond Light Source, Oxfordshire, and were subsequently indexed, integrated, and scaled to 2.0-Å resolution using the program XDS [45,46]. Diffraction data for the crystal of *Mvu*TFIIB^{Δ145} mini-intein were collected in a single pass on beamline ID30A-3 at the European Synchrotron Research Facility, Grenoble, and were subsequently indexed, integrated, and scaled to 2.5-Å resolution [47]. Crystal parameters and data processing statistics are listed in Table 1.

Structure determination and refinement

The structures of *Mja*TFIIB^{Δ155} and *Mvu*TFIIB^{Δ145} were solved by molecular replacement. The search model used for *Mja*TFIIB^{Δ155} was based on the coordinate of the intein part of PI-Tkoll (PDB ID: 2cw8). Since the intein is present in this structure as two separate segments joined by the extein, a model of the single-chain target protein was constructed with the program Sculptor [48]. The sequence of this model was mutated to that of *Mja*TFIIB^{Δ155}, and the resulting coordinates were subjected to restrained molecular dynamics with Rosetta. Since the sequence identity between *Mja*TFIIB and the PI-Tkoll is only 31%, molecular replacement runs that used either this starting model, or unmodified and modified structures of several inteins, were initially unsuccessful. A correct solution was only obtained with the help of the program MR_Rosetta coupled to the Phenix package [49,50]. The model was adjusted with Coot followed by rounds of refinement with Phenix [50,51]. The quality of the final structure was validated by the MolProbity webserver (Table 1) [52].

The structure of molecule A of *Mja*TFIIB intein, with the sequence adjusted with Sculptor to that of *Mvu*TFIIB, was used as a starting model for molecular replacement. The structure was solved with Phenix

and improved with MR_Rosetta, yielding a solution consisting of two molecules in the asymmetric unit, with the *R* of 0.286 and *R*_{free} of 0.377, with several loops still missing [49,50]. Further refinement was performed with Refmac5 from CCP4 package, and the model was rebuilt with Coot and validated with MolProbity (Table 1) [51–54].

Homology modeling of the full-length *Mja*TFIIB intein

The three-dimensional model of the full-length *Mja*TFIIB intein was built by SwissModel online server[‡] using PI-*Pful* (PDB ID: 1dq3) as a template model [55].

Accession numbers

Coordinates and structure factors have been deposited in the PDB with accession number 5o9j for the *Mja*TFIIB intein, 5o9i for the *Mvu*TFIIB intein.

Supplementary data to this article can be found online at <https://doi.org/10.1016/j.jmb.2017.10.016>.

Acknowledgments

We thank B. Haas and S. Jääskeläinen for technical help in preparation of proteins and plasmids. We thank S. Mäki and Dr. K. Kogan for technical help at the crystallization facility. This work was supported in part by the Academy of Finland (137995, 1277335) and Biocenter Finland for the crystallization and NMR facilities at the Institute of Biotechnology, by the Intramural Research Program of the National Institutes Health, National Cancer Institute, Center for Cancer Research, and with Federal funds from the National Cancer Institute, NIH, under Contract No. HHSN261200800001E (to M.L.). The content of this publication is solely the responsibility of the authors and does not necessarily represent the official views or policies of the Department of Health and Human Services, nor does the mention of trade names, commercial products, or organizations imply endorsement by the US Government.

Received 19 June 2017;

Received in revised form 29 September 2017;

Accepted 12 October 2017

Available online 18 October 2017

Keywords:

inteins;
protein splicing;
homing endonuclease;
horizontal gene transfer

⁴Present address: J. Oeemig, VIB Center for Structural Biology, Vlaams Instituut voor Biotechnologie (VIB), Vrije Universiteit Brussel (VUB), Brussels, Belgium.

⁵Present address: D. Zhou, Blood Research Institute, Blood Center of Wisconsin, Milwaukee, WI 53226, USA.

†<http://www.biocenter.helsinki.fi/bi/xray/automation/services.html>.

‡<https://swissmodel.expasy.org/>.

Abbreviations used:

Mja, *Methanococcus jannaschii*; *Mvu*, *Methanocaldococcus vulcanius* M7; HEN, homing endonuclease; HINT, Hedgehog/INTein; HGT, horizontal gene transfer; PDB, Protein Data Bank; GB1, B1 domain of IgG binding protein G; IMAC, immobilized metal ion affinity chromatography; iPAS, intein-mediated protein alternative splicing.

References

- [1] H. Keren, G. Lev-Maor, G. Ast, Alternative splicing and evolution: diversification, exon definition and function, *Nat. Rev. Genet.* 11 (2010) 345–355.
- [2] D.L. Black, Protein diversity from alternative splicing: a challenge for bioinformatics and post-genome biology, *Cell* 103 (2000) 367–370.
- [3] A.S. Aranko, J.S. Oeemig, T. Kajander, H. Iwai, Intermolecular domain swapping induces intein-mediated protein alternative splicing, *Nat. Chem. Biol.* 9 (2013) 616–622.
- [4] J.P. Gogarten, A.G. Senejani, O. Zhaxybayeva, L. Olendzenski, E. Hilario, Inteins: structure, function, and evolution, *Annu. Rev. Microbiol.* 56 (2002) 263–287.
- [5] H. Paulus, Protein splicing and related forms of protein autoprocessing, *Annu. Rev. Biochem.* 69 (2000) 447–496.
- [6] M. Kawasaki, Y. Satow, Y. Ohya, Y. Anraku, Protein splicing in the yeast Vma1 protozyme: evidence for an intramolecular reaction, *FEBS Lett.* 412 (1997) 518–520.
- [7] H. Wu, Z. Hu, X.Q. Liu, Protein trans-splicing by a split intein encoded in a split DnaE gene of *Synechocystis* sp. PCC6803, *Proc. Natl. Acad. Sci. U. S. A.* 95 (1998) 9226–9231.
- [8] O. Novikova, P. Jayachandran, D.S. Kelley, Z. Morton, S. Merwin, N.I. Topilina, et al., Inteins: structure, function, and evolution, *Annu. Rev. Microbiol.* 56 (2002) 263–287.
- [9] K.S. Swithers, S.M. Soucy, J.P. Gogarten, The role of reticulate evolution in creating innovation and complexity, *Int. J. Evol. Biol.* 2012 (2012), 418964.
- [10] B.P. Callahan, N.I. Topilina, M.J. Stanger, P. Van Roey, M. Belfort, Structure of catalytically competent intein caught in a redox trap with functional and evolutionary implications, *Nat. Struct. Mol. Biol.* 18 (2011) 630–633.
- [11] N.I. Topilina, O. Novikova, M. Stanger, N.K. Banavali, M. Belfort, Post-translational environmental switch of RadA activity by extein–intein interactions in protein splicing, *Nucleic Acids Res.* 43 (2015) 6631–6648.
- [12] N.I. Topilina, G.M. Green, P. Jayachandran, D.S. Kelley, M. Stanger, C.L. Piazza, S. Nayak, M. Belfort, SufB intein of *Mycobacterium tuberculosis* as a sensor for oxidative and nitrosative stresses, *Proc. Natl. Acad. Sci. U. S. A.* 112 (2015) 10348–10353.
- [13] T.M. Hall, J.A. Porter, K.E. Young, E.V. Koonin, P.A. Beachy, D.J. Leahy, Crystal structure of a Hedgehog autoprocessing domain: homology between Hedgehog and self-splicing proteins, *Cell* 91 (1997) 85–97.
- [14] S. Nogami, Y. Satow, Y. Ohya, Y. Anraku, Probing novel elements for protein splicing in the yeast Vma1 protozyme: a study of replacement mutagenesis and intragenic suppression, *Genetics* 147 (1997) 73–85.
- [15] F.S. Gimble, J. Thorner, Homing of a DNA endonuclease gene by meiotic gene conversion in *Saccharomyces cerevisiae*, *Nature* 357 (1992) 301–306.
- [16] V. Derbyshire, D.W. Wood, W. Wu, J.T. Dansereau, J.Z. Dalgaard, M. Belfort, Genetic definition of a protein-splicing domain: functional mini-inteins support structure predictions and a model for intein evolution, *Proc. Natl. Acad. Sci. U. S. A.* 94 (1997) 11466–11471.
- [17] T. Klabunde, S. Sharma, A. Telenti, W.R. Jacobs, J.C. Sacchettini, Crystal structure of GyrA intein from *Mycobacterium xenopi* reveals structural basis of protein splicing, *Nat. Struct. Biol.* 5 (1998) 31–36.
- [18] A.S. Aranko, J.S. Oeemig, D. Zhou, T. Kajander, A. Wlodawer, H. Iwai, Structure-based engineering and comparison of novel split inteins for protein ligation, *Mol. Biosyst.* 10 (2014) 1023–1034.
- [19] H. Wu, M.Q. Xu, X.Q. Liu, Protein trans-splicing and functional mini-inteins of a cyanobacterial dnaB intein, *Biochim. Biophys. Acta* 1387 (1998) 422–432.
- [20] A. Barzel, A. Naor, E. Privman, M. Kupiec, U. Gophna, Homing endonucleases residing within inteins: evolutionary puzzles awaiting genetic solutions, *Biochem. Soc. Trans.* 39 (2011) 169–173.
- [21] V. Koufopanou, A. Burt, Degeneration and domestication of a selfish gene in yeast: molecular evolution versus site-directed mutagenesis, *Mol. Biol. Evol.* 22 (2005) 1535–1538.
- [22] S. Ellilä, J.M. Jurvansuu, H. Iwai, Evaluation and comparison of protein splicing by exogenous inteins with foreign exons in *Escherichia coli*, *FEBS Lett.* 585 (2011) 3471–3477.
- [23] R. Mizutani, S. Nogami, M. Kawasaki, Y. Ohya, Y. Anraku, Y. Satow, Protein-splicing reaction via a thiazolidine intermediate: crystal structure of the VMA1-derived endonuclease bearing the N and C-terminal propeptides, *J. Mol. Biol.* 316 (2002) 919–929.
- [24] K. Ichiyana, Y. Ishino, M. Ariyoshi, K. Komori, K. Morikawa, Crystal structure of an archaeal intein-encoded homing endonuclease PI-*Pful*, *J. Mol. Biol.* 300 (2000) 889–901.
- [25] C.M. Moure, F.S. Gimble, F.A. Quiocho, Crystal structure of the intein homing endonuclease PI-*Scel* bound to its recognition sequence, *Nat. Struct. Biol.* 9 (2002) 764–770.
- [26] H. Matsumura, H. Takahashi, T. Inoue, T. Yamamoto, H. Hashimoto, M. Nishioka, et al., Crystal structure of intein homing endonuclease II encoded in DNA polymerase gene from hyperthermophilic archaeon *Thermococcus kodakaraensis* strain KOD1, *Proteins* 63 (2006) 711–715.
- [27] J.S. Oeemig, D. Zhou, T. Kajander, A. Wlodawer, H. Iwai, NMR and crystal structures of the *Pyrococcus horikoshii* RadA intein guide a strategy for engineering a highly efficient and promiscuous intein, *J. Mol. Biol.* 421 (2012) 85–99.
- [28] Y. Okuda, D. Sasaki, S. Nogami, Y. Kaneko, Y. Ohya, Y. Anraku, Occurrence, horizontal transfer and degeneration of VDE intein family in *Saccharomycete* yeasts, *Yeast* 20 (2003) 563–573.
- [29] K.S. Swithers, A.G. Senejani, G.P. Fournier, J.P. Gogarten, Conservation of intron and intein insertion sites: implications

- for life histories of parasitic genetic elements, *BMC Evol. Biol.* 9 (2009) 303.
- [33] M. Cronin, M.J. Coolbaugh, D. Nellis, J. Zhu, D.W. Wood, R. Nussinov, et al., Dynamics differentiate between active and inactive inteins, *Eur. J. Med. Chem.* 91 (2015) 51–62.
- [34] Z. Du, Y. Liu, D. Ban, M.M. Lopez, M. Belfort, C. Wang, Backbone dynamics and global effects of an activating mutation in minimized Mtu RecA inteins, *J. Mol. Biol.* 400 (2010) 755–767.
- [35] J.M. Wenzlau, R.J. Saldanha, R.A. Butow, P.S. Perlman, A latent intron-encoded maturase is also an endonuclease needed for intron mobility, *Cell* 56 (1989) 421–430.
- [36] J.P. Gogarten, E. Hilario, Inteins, introns, and homing endonucleases: recent revelations about the life cycle of parasitic genetic elements, *BMC Evol. Biol.* 6 (2006) 94.
- [37] F.B. Perler, A natural example of protein trans-splicing, *Trends Biochem. Sci.* 24 (1999) 209–211.
- [38] S. Pietrovski, Intein spread and extinction in evolution, *Trends Genet.* 17 (2001) 465–472.
- [39] A.S. Aranko, A. Wlodawer, H. Iwai, Nature's recipe for splitting inteins, *Protein Eng. Des. Sel.* 27 (2014) 263–271.
- [40] C.W. Lennon, M. Belfort, Inteins, *Curr. Biol.* 27 (2017) R204–R206.
- [41] A.T. Brünger, The free *R* value: a novel statistical quantity for assessing the accuracy of crystal structures, *Nature* 355 (1992) 472–475.
- [42] M. Muona, A.S. Aranko, H. Iwai, Segmental isotopic labelling of a multidomain protein by protein ligation by protein trans-splicing, *Chembiochem* 9 (2008) 2958–2961.
- [43] F. Guerrero, A. Ciragan, H. Iwai, Tandem SUMO fusion vectors for improving soluble protein expression and purification, *Protein Expr. Purif.* 116 (2015) 42–49.
- [44] R. Cudney, S. Patel, K. Weisgraber, Y. Newhouse, A. McPherson, Screening and optimization strategies for macromolecular crystal growth, *Acta Crystallogr. D Biol. Crystallogr.* 50 (1994) 414–423.
- [45] P. Theveneau, R. Baker, R. Barrett, A. Beteva, M.W. Bowler, P. Carpentier, et al., The upgrade programme for the structural biology beamlines at the European Synchrotron Radiation Facility—high throughput sample evaluation and automation, *J. Phys. Conf. Ser.* 425 (2013), 012001. <https://doi.org/10.1088/1742-6596/425/1/012001>.
- [46] W. Kabsch, XDS, *Acta Crystallogr. D* 66 (2010) 125–132.
- [47] D.R. Allan, S.P. Collins, G. Evans, D. Hall, K. McAuley, R.L. Owen, et al., Status of the crystallography beamlines at Diamond Light Source, *Eur. Phys. J. Plus* 130 (2015) 56.
- [48] G. Bunkóczi, R.J. Read, Improvement of molecular-replacement models with *Sculptor*, *Acta Crystallogr. D Biol. Crystallogr.* 67 (2011) 303–312.
- [49] F. DiMaio, T.C. Terwilliger, R.J. Read, A. Wlodawer, G. Oberdorfer, U. Wagner, et al., Increasing the radius of convergence of molecular replacement by density and energy guided protein structure optimization, *Nature* 473 (2011) 540–543.
- [50] P.D. Adams, R.W. Grosse-Kunstleve, L.W. Hung, T.R. Ioerger, A.J. McCoy, N.W. Moriarty, et al., PHENIX: building new software for automated crystallographic structure determination, *Acta Crystallogr. D* 58 (2002) 1948–1954.
- [51] P. Emsley, B. Lohkamp, W.G. Scott, K. Cowtan, Features and development of Coot, *Acta Crystallogr. D* 66 (2010) 486–501.
- [52] V.B. Chen, W.B. Arendall III, J.J. Headd, D.A. Keedy, R.M. Immormino, G.J. Kapral, et al., MolProbity: all-atom structure validation for macromolecular crystallography, *Acta Crystallogr. D* 66 (2010) 12–21.
- [53] M.D. Winn, C.C. Ballard, K.D. Cowtan, E.J. Dodson, P. Emsley, P.R. Evans, R.M. Keegan, et al., Overview of the CCP4 suite and current developments, *Acta Crystallogr. D* 67 (2011) 235–242.
- [54] G.N. Murshudov, P. Skubak, A.A. Lebedev, N.S. Pannu, R.A. Steiner, R.A. Nicholls, et al., REFMAC5 for the refinement of macromolecular crystal structures, *Acta Crystallogr. D* 67 (2011) 355–367.
- [55] K. Arnold, L. Bordoli, J. Kopp, T. Schwede, The SWISS-MODEL workspace: a Web-based environment for protein structure homology modelling, *Bioinformatics* 22 (2006) 195–201.